


The formation of a neutral manganese(III) complex containing a tetradentate Schiff base and a ketone – synthesis and characterization

Agata Bartyzel & Agnieszka A. Kaczor


To cite this article: Agata Bartyzel & Agnieszka A. Kaczor (2015) The formation of a neutral manganese(III) complex containing a tetradentate Schiff base and a ketone – synthesis and characterization, Journal of Coordination Chemistry, 68:20, 3701-3717, DOI: 10.1080/00958972.2015.1073268

To link to this article: <http://dx.doi.org/10.1080/00958972.2015.1073268>

 View supplementary material 

 Accepted author version posted online: 21 Jul 2015.
Published online: 20 Aug 2015.

 Submit your article to this journal 

 Article views: 115

 View related articles 

 View Crossmark data 

The formation of a neutral manganese(III) complex containing a tetradentate Schiff base and a ketone – synthesis and characterization

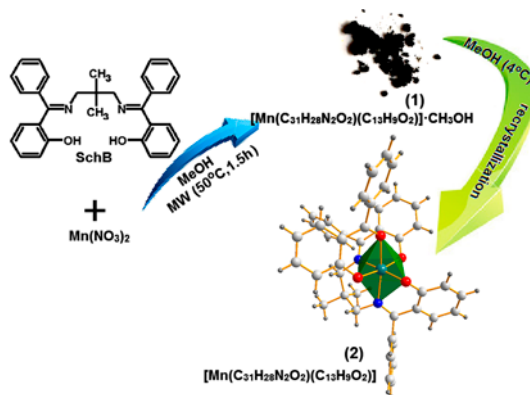
AGATA BARTYZEL*† and AGNIESZKA A. KACZOR‡§

†Faculty of Chemistry, Department of General and Coordination Chemistry, Maria Curie-Skłodowska University, Lublin, Poland

‡Faculty of Pharmacy with Division of Medical Analytics, Department of Synthesis and Chemical Technology of Pharmaceutical Substances with Computer Modelling Lab, Medical University of Lublin, Lublin, Poland

§Department of Pharmaceutical Chemistry, School of Pharmacy, University of Eastern Finland, Kuopio, Finland

(Received 16 October 2014; accepted 10 June 2015)



2-Benzoylphenolato-(2,2'-((2,2-dimethylpropane-1,3-diyl)bis((nitriolo)(phenylmethylidene)))diphenolato-manganese(III) methanol solvate, $[\text{Mn}(\text{C}_{31}\text{H}_{28}\text{N}_2\text{O}_2)(\text{C}_{13}\text{H}_9\text{O}_2)] \cdot \text{CH}_3\text{OH}$ (**1**), was synthesized and characterized by FTIR, UV–vis, TG–FTIR, TG/DSC, molar conductivity, magnetic moment measurement, and quantum chemical calculations. During the synthesis, partial hydrolysis of ligand is observed. The compound was obtained as amorphous, dark-brown powder. The effects of organic solvents of various polarities on the UV–vis spectra of ligands and complex were investigated. In addition, the IR and UV–vis spectra were also calculated and compared with the experimental data. A single crystal for analysis was obtained by dissolving the amorphous complex in methanol, and slow evaporation of solvent at 4 °C. Single-crystal X-ray analysis indicated that the methanol molecules are not incorporated into the crystal lattice after the recrystallization process ($[\text{Mn}(\text{C}_{31}\text{H}_{28}\text{N}_2\text{O}_2)(\text{C}_{13}\text{H}_9\text{O}_2)]$ (**2**)). In the structure Mn(III) is surrounded by two nitrogens and four oxygens of deprotonated Schiff base and α -hydroxy ketone ligands, and adopts a distorted octahedral geometry.

Keywords: Tetradentate Schiff base; Manganese(III) complex; Crystal structure; Spectral analysis; Thermal analysis; Quantum chemical calculations

*Corresponding author. Emails: adaxe13@wp.pl; agata.bartyzel@poczta.umcs.lublin.pl

1. Introduction

The chemistry of manganese has been the subject of many studies, since this metal is a constituent or a cofactor for a number of important enzymes, e.g. superoxide dismutase, catalase, oxalate oxidase, arginase, cholinesterase, phosphoglucomutase, etc. [1]. There is further interest in the study of manganese compounds due to their magnetic [2], photoluminescence [3], antifungal, antibacterial [4], and catalytic properties [5]. Special attention has been paid to the studies of manganese complexes with ligands containing N and/or O donors, due to their interesting coordination chemistry [3(b), 6] and their role in inorganic biochemistry [6(a, c, and h), 7], catalysis [3(b), 6(f–i), 7(e), 8], and optical [6(h), 9], or magnetic materials [3(b), 6(c, j–k), 10]. For these reasons, synthesis and characterization of manganese complexes with polydentate Schiff base ligands, particularly with salen-type derivatives (tetradentate, N_2O_2), have been extensively examined [1(c), 2(a), 6(f–i), 7(a, e), 8(a–d)].

In this paper, we present the structure of a manganese(III) complex with mixed ligands. To the best of our knowledge, few similar structures, i.e. containing salen-type Schiff base and aldehyde- or ketone-phenolate anions, have been described [11]. The complex presented here is the first described structure of this kind containing a Mn(III) center. Similar complexes, but containing Co(III), were prepared by Fukuhara *et al.* in the reaction of previously synthesized Co(II)-Schiff base compounds and appropriate phenyl aldehyde or ketone ligands [11(a)]. Gupta and co-workers synthesized a mononuclear, neutral Co(III) complex using the direct (where both ligands, a ketone and Schiff base, were used) and template methods [11(b)]. In our case, similar to the synthesis of Co(III) complex reported by Kia *et al.* [11(c)], the Mn(III) complex was prepared by the direct method using manganese(II) salt and Schiff base ligand in 1 : 1 ratio. During synthesis, the partial hydrolysis process is observed and the final complex contains a tetradentate Schiff base and a ketone coordinated to Mn(III). We report synthesis, thermal and spectroscopic characterization of the mononuclear manganese(III) complex ($Mn(C_{31}H_{28}N_2O_2)(C_{13}H_9O_2) \cdot CH_3OH$ (**1**)) with a tetradentate Schiff base and a ketone (scheme 1). Complex **1** has also been characterized with molar conductivity and magnetic moment studies. The molecular structure of the recrystallized complex ($[Mn(C_{31}H_{28}N_2O_2)(C_{13}H_9O_2)]$ (**2**)) was also determined by X-ray crystallography. Furthermore, quantum chemical calculations were performed to address the structure of **2** and to compute IR and UV–vis spectra.

2. Experimental

2.1. Materials

The 2,2-dimethyl-1,3-propanediamine and 2-hydroxybenzophenone (K) (scheme 1) used for preparation of a Schiff base were obtained from Aldrich Chemical Company. The metal salt $Mn(NO_3)_2 \cdot 4H_2O$ was purchased from Merck. The organic solvents (MeOH, EtOH, ACN, DMF, and THF) were purchased from Polish Chemical Reagents in Gliwice (Poland). All solvents and chemicals were reagent grade and used without purification.

2.2. Synthesis

2.2.1. Preparation of 2,2'-((2,2-dimethylpropane-1,3-diyl)bis((nitrilo)(phenylmethylidyne))-diphenol (SchB). The Schiff base (scheme 1) was synthesized according to the method described in previous papers [12]. A solution of 10 mmol 2-hydroxybenzophenone and 5 mmol 2,2-dimethyl-1,3-propanediamine in 60 mL of methanol was refluxed for 5 h. The excess of the solvent (*ca.* 50 mL) was then evaporated. After cooling to 4 °C, a yellow solid was produced. The polycrystalline product was collected by filtration, washed with methanol, and dried (74.5% yields). Elemental analysis of $C_{31}H_{30}N_2O_2$, Calcd (%): C, 80.49; H, 6.54; N, 6.06. Found: C, 80.41; H, 6.63; N, 5.98.

2.2.2. Preparation of 1 and 2. A mixture of stoichiometric amounts of manganese(II) nitrate (1 mmol) and Schiff base (1 mmol) in 15 mL of methanol was placed in a 100-mL Teflon vessel. The reaction mixture was heated to 50 °C for 20 min and kept at that temperature for 1.5 h. The content of the vessels was stirred during the whole time of the synthesis and then cooled. The solution was left in air allowing complete evaporation of solvent. A solid, dark-brown product (2-benzoylphenolato-(2,2'-((2,2-dimethylpropane-1,3-diyl)bis((nitrilo)(phenyl-methylidyne))-diphenolato-manganese(III) methanol solvate (1)) was washed with cold methanol until pH of the filtrate was 5. The residue was dried in air and later recrystallized from methanol. The yield of the purified complex was 44.6%. Elemental analysis of $[Mn(C_{31}H_{28}N_2O_2)(C_{13}H_9O_2)] \cdot CH_3OH$ ($M = 744.75 \text{ g mol}^{-1}$). Calcd (%): C, 72.57; H, 5.55; N, 3.76. Found: C, 72.19; H, 5.41; N, 3.78. After dissolving the pure recrystallized compound (50 mg) in methanol and slowly evaporating the solvent at 4 °C, a few single crystals suitable for X-ray analysis were obtained (2-benzoylphenolato(2,2'-((2,2-dimethylpropane-1,3-diyl)bis((nitrilo)(phenyl-methylidyne))-diphenolato-manganese(III) (2)). The yield of 2 was 11.6%. Elemental analysis of $[Mn(C_{31}H_{28}N_2O_2)(C_{13}H_9O_2)]$ ($M = 712.71 \text{ g mol}^{-1}$). Calcd (%): C, 74.15; H, 5.23; N, 3.93. Found: C, 74.43; H, 5.12; N, 4.01.

2.3. Methods and physical measurements

The microwave oven used in this study was a CEM MARS-5 system equipped with temperature and pressure controllers. Elemental analysis for C, H, and N was performed using a Perkin-Elmer CHN 2400 analyzer. Magnetic susceptibility measurement was conducted at 295 K using a magnetic susceptibility balance MSB-MKI, Sherwood Scientific Ltd, Cambridge. The data were corrected for diamagnetic susceptibilities [13]. The effective magnetic moment was calculated from the equation $\mu_{\text{eff}} = 2.828(\chi_{\text{cor}}T)^{1/2}$. The molar conductivities were measured at 25 °C using a PHYWE 13701.93 conductivity meter. The infrared spectra were obtained using a Thermo Scientific Nicolet 6700 FTIR with a Smart iTR diamond ATR accessory. The data were collected between 4000 and 600 cm^{-1} with a resolution of 4 cm^{-1} for 16 scans (figures S1–S4, see online supplemental material at <http://dx.doi.org/10.1080/00958972.2015.1073268>). The UV–vis spectra were obtained by a Genesys 10s spectrophotometer (Thermo Scientific) using 1.0 cm quartz cells. Thermal stability and decomposition of the analyzed complexes were determined by a Setaram Setsys 16/18 derivatograph, recording TG, DTG, and DSC curves. The samples [5.33 mg (1) and 2.65 mg (2)] were heated in a ceramic crucible between 30 and 850 °C in flowing air

atmosphere ($v = 1 \text{ dm}^3 \text{ h}^{-1}$) with a heating rate of $10 \text{ }^\circ\text{C min}^{-1}$. The TG–FTIR of the title compound was recorded using the TGA Q5000 analyzer TA Instruments, New Castle, Delaware, USA, interfaced to the Nicolet 6700 FTIR spectrophotometer (Thermo Scientific). About 16.36 mg of **1** was put in an open ceramic crucible and heated from 30 to $1000 \text{ }^\circ\text{C}$. The analysis was carried out at a heating rate of $20 \text{ }^\circ\text{C min}^{-1}$ under nitrogen at a flow rate of 50 mL min^{-1} . To reduce the possibility of gasses condensing along the transfer line, the temperature in the gas cell and transfer line was set to 250 and $240 \text{ }^\circ\text{C}$, respectively. Gas analysis was performed by matching the spectra against those from the spectrum library Nicolet TGA Vapor Phase of the software Ominic together with the literature sources.

2.4. X-ray crystallographic studies

Single-crystal diffraction data were collected using an Oxford Diffraction Xcalibur CCD diffractometer with graphite-monochromated MoK_α radiation ($\lambda = 0.71073 \text{ \AA}$). The temperature for the experiment was maintained at 100 K with an Oxford Cryosystem N_2 gas-stream cooling device. The programs CrysAlis CCD and CrysAlis Red [14(a)] were used for data collection, cell refinement, and data reduction. A semi-empirical absorption–correction based on the intensities of equivalent reflections was applied, and the data were corrected for Lorentz and polarization effects. The structure was solved by direct methods using SHELXS-2013 and refined by full-matrix least squares on F^2 using SHELXL-2013 [14(b)], both operating under WinGX [14(c)]. All non-hydrogen atoms were refined with anisotropic displacement parameters. Hydrogens residing on carbon were positioned geometrically and refined applying the riding model [$\text{C–H} = 0.95\text{--}0.98 \text{ \AA}$ and with $U_{\text{iso}}(\text{H}) = 1.2$ or $1.5 U_{\text{eq}}(\text{C})$]. The molecular plots were drawn with ORTEP3 for Windows [14(d)], Mercury [14(e)] and Diamond [14(f)]. The geometrical calculations were performed using the PLATON program [14(g)].

2.5. Quantum chemical calculations

The energy and geometry of the ketone, Schiff base, and **2** were optimized using the Hartree–Fock and B3LYP DFT [15(a) and (b)] methods and 6-311++G(3df,3pd) basis set of Gaussian09 [15(c)]. The simulations of manganese compounds, in particular carried out using DFT methods, often reveal a very poor convergence of the iterative procedure for finding the solution of the Kohn–Sham equations [15(d)]. Thus, we employed a step-by-step procedure of complex optimization, starting with the semi-empirical PM6 method, then HF/6-31G(d,p) optimization and finally HF/6-311++G(3df,3pd) and B3LYP/6-311++G(3df,3pd). The selection of the final basis set was a compromise between the accuracy of the computations and the available resources. Visualization of data was performed with Discovery Studio v. 3.1 [15(e)] and Gabedit v. 2.4.8 [15(f)]. Next, IR spectra were computed for the ketone, Schiff base, and complex using the Hartree–Fock and B3LYP method and 6-311++G(3df,3pd) basis set of Gaussian09. Preliminary vibrational band assignment was performed using ChemCraft v. 1.7 software [15(g)] and based on the literature (see table 1, Supplementary data). Moreover, the computed vibrational frequencies have been unambiguously assigned by means of the potential energy distribution analysis of all the fundamental vibration modes using VEDA 4 program [15(h–i)] as described previously [15(j–l)] (tables S2–S4, Supplementary data). Chemissian v. 4.01 [15(m)] was used for visualization of UV–vis spectra.

Table 1. Molar conductivity data of **1** (concentration 1.0×10^{-3} , $T = 25$ °C).

Solvent	Complex $\Lambda_m [\Omega^{-1} \text{ cm}^2 \text{ mol}^{-1}]$
MeOH	92.30
EtOH	39.40
DMF	78.80
ACN	54.80
THF	0.85

3. Results and discussion

The most common synthesis of metal complexes is the reaction of metal salts with Schiff base ligand (direct method) or with ketone/aldehyde and amine (template method) in a refluxing organic solvent [11, 16]. Here, we applied the microwave technique because it allows improving product yields, reducing reaction times, making it appropriate for green chemistry, and energy-saving processes. The new complex of manganese(III) was synthesized by the reaction of Mn(II) salt and SchB. During the synthesis, a partial hydrolysis of Schiff base ligand is observed. As a result, one product of hydrolysis (ketone) is bound to the metal center to give a complex $[\text{Mn}(\text{C}_{31}\text{H}_{28}\text{N}_2\text{O}_2)(\text{C}_{13}\text{H}_9\text{O}_2)] \cdot \text{CH}_3\text{OH}$ (**1**). Complex **1** is stable at room temperature, both isolated and in solution. The room temperature magnetic moment of the complex is $5.17 \mu_B$, confirming that Mn^{2+} was oxidized to Mn^{3+} . The value is close to the literature ones (4.80 – $5.00 \mu_B$) for high-spin ($S = 2$) magnetically dilute d^4 manganese(III) ion with an octahedral geometry. It is characteristic of monomeric Mn(III) complexes, where metal ion indicates little or no antiferromagnetic interaction [6(j–k), 7(e)]. X-ray structure analysis confirmed the formation of a monomeric complex. The molar conductivities of **1** were measured in different solvents (table 1) at $10^{-3} \text{ mol L}^{-1}$. The molar conductivity of **1** performed in THF ($0.85 \Omega^{-1} \text{ cm}^2 \text{ mol}^{-1}$) indicates the non-electrolytic nature. In the case of complex solution in ACN, the molar conductivity is $54.80 \Omega^{-1} \text{ cm}^2 \text{ mol}^{-1}$. This value is lower than that characteristic of uni-univalent (1 : 1) electrolyte (120 – $160 \Omega^{-1} \text{ cm}^2 \text{ mol}^{-1}$) [17], but it indicates that complex is partially dissociated. In remaining solvents, the complex behaves as a uni-univalent (1 : 1) electrolyte [17] which also indicate that in solution ketone ligand coordinating to Mn(III) ion is replaced by appropriate solvent molecules.

3.1. Infrared spectra

In the solid state, SchB exists in the enolimine form [18]. Similar to previous reports [16], the $\nu(\text{O-H})$ band is not observed due to the presence of a strong intramolecular hydrogen bond $\text{O-H} \cdots \text{N}$ [19]. For a similar reason, $\nu(\text{O-H})$ band is not detected in the spectrum of the ketone because of the strong intramolecular hydrogen bonds $\text{O-H} \cdots \text{O}$ [20]. The presence of intramolecular hydrogen bonds in SchB and K ligands influences the electron density of the C=N and C=O groups, which causes the corresponding stretching vibrations [$\nu(\text{C=N})$ and $\nu(\text{C=O})$] to be observed at lower frequency (at 1596 and 1626 cm^{-1} , respectively). All these results are consistent with the crystal structures and are in agreement with the literature [18–20]. In spectra of **1** and **2**, $\nu(\text{C=N})$ band occurs at similar frequencies compared to the

free Schiff base, i.e. 1595 cm^{-1} (for **1**) and 1594 cm^{-1} (for **2**). In the case of $\nu(\text{C}=\text{O})$ band, coordination of the carbonyl oxygen to Mn(III) has stronger influence on electron density of the C=O and shifts the band to a lower wavelength (1620 cm^{-1} for **1** and 1608 cm^{-1} for **2**). Similar shifts to lower wavenumber have been reported in the mixed ligand complexes of Sr (II) and Ba(II) containing 2-hydroxybenzophenone [20(a)]. The Schiff base and ketone ligand also coordinate Mn(III) ion via deprotonated phenolic oxygen. In analogy to other complexes, where a metal center is coordinated via the phenoxy group [16, 21], the phenolic O–H deformation bands (1335 , 1221 , and 1202 cm^{-1} for K and 1331 , 1218 , and 1200 cm^{-1} for SchB) do not occur in the spectrum of complexes. In the case of **1**, a molecule of methanol is also included in the structure. The bands connected with the presence of CH_3OH in **1** are observed at 3368 cm^{-1} [$\nu(\text{O}-\text{H})$], 1307 cm^{-1} [$\nu(\text{C}-\text{O})$], and 1095 cm^{-1} [$\nu(\text{C}-\text{O})$]. The remaining bands characteristic of both ligands and **1** and **2** are listed in table S1 (Supplementary data).

The calculated “raw” HF and DFT frequencies are usually significantly overestimated in comparison to the experimental values because of the lack of electron correlation, an insufficient basis set and anharmonicity [22(a) and (b)]. Thus, we used the scaling factors reported in the literature to enhance raw results. The raw IR spectra were scaled with 0.9010 scaling factor for HF/6-311++G(3df,3pd) calculations and with 0.9604 scaling factor for B3LYP/6-311++G(3df,3pd) calculations [22(c) and (d)]. Owing to the scaling procedure, we obtained good agreement between the experimental and calculated raw frequencies (tables S2–S4, Supplementary data).

3.2. Crystal structure

The molecular structure of **2** is displayed in figure 1. The crystallographic and refinement data for **2** are summarized in table 2. Selected bond distances and angles are listed in table 3; the hydrogen bond parameters are given in table 4. RMSD measured on heavy atoms between the X-ray structure and HF/6-311++G(3df,3pd) was 0.9368 \AA and between the crystal-ray structure and B3LYP/6-311++G(3df,3pd) was 0.5738 \AA . The superposition of X-ray structure, HF/6-311++G(3df,3pd) optimized structure, and B3LYP/6-311++G(3df,3pd) optimized structure is shown in figure S5 (Supplementary data). The largest differences between X-ray and computed structures were found for the coordination bonds around the central Mn. However, the overall geometry of X-ray and computed structures is similar as indicated by low RMSD values (1.4587 \AA between the crystal structure and HF/6-311++G(3df,3pd) optimized structure and 0.9846 \AA between the crystal structure and B3LYP/6-311++G(3df,3pd) optimized structure) and high correlation coefficients R^2 (0.9615 for bonds, 0.9427 for angles and 0.9512 for torsion angles between the crystal structure and HF/6-311++G(3df,3pd) optimized structure; 0.9889 for bonds, 0.9777 for angles and 0.9623 for torsion angles between the crystal structure and B3LYP/6-311++G(3df,3pd) optimized structure). During slow recrystallization, methanol molecules are not included into the crystal structure of **2**. Complex **2** crystallizes in the monoclinic space group $P2_1/n$. The Mn center is in an octahedral environment consisting of O1, O2, N1, and N2 donors (two phenoxo oxygens and two imine nitrogens) from the Schiff base ligand and O3 and O4 donors (phenoxo and carbonyl oxygens) from the ketone. The manganese ion has a tetragonally elongated octahedral coordination geometry (see figure 2) which is typical of the Jahn–Teller distorted d^4 high spin Mn(III) [1(c), 6(c) and (i), 10(b), 16, 23]. The equatorial plane is formed by three phenolate oxygens (both ligands) and one nitrogen

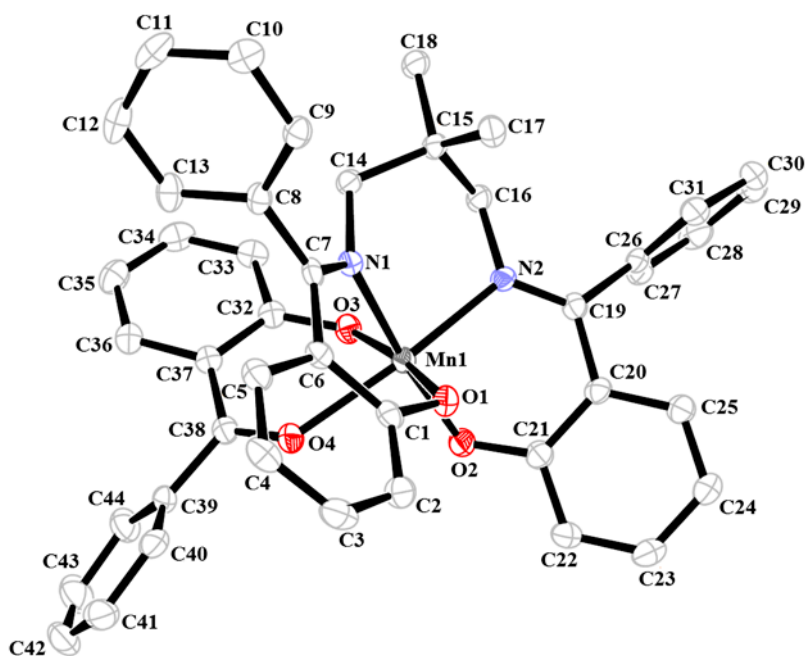


Figure 1. ORTEP view with the atom numbering scheme of **2**. Displacement ellipsoids are drawn at the 50% probability level. All hydrogens are omitted for clarity.

Table 2. Crystal data and structure refinement for **2**.

Formula	$[\text{Mn}(\text{C}_{31}\text{H}_{28}\text{N}_2\text{O}_2)(\text{C}_{13}\text{H}_9\text{O}_2)]$
Formula weight	712.70
Temperature (K)	100(2)
Crystal system	Monoclinic
Space group	$P2_1/n$
a (Å)	9.7096(3)
b (Å)	14.6783(6)
c (Å)	24.8962(7)
β (°)	95.940(3)
Volume (Å ³)	3529.2(2)
Z	4
Calcd density (g cm ⁻³)	1.341
μ (mm ⁻¹)	0.421
Absorption correction	Multi-scan
$F(0\ 0\ 0)$	1488
Crystal size (mm)	0.20 × 0.10 × 0.10
θ range (°)	2.59–27.48
Index ranges	–12 ≤ h ≤ 12 –19 ≤ k ≤ 19 –30 ≤ l ≤ 32
Reflections collected/unique	29,325/8093
R_{int}	0.0564
Data/restraints/parameters	6239/0/368
Goof on F^2	0.999
Final R indices [$I > 2\sigma(I)$]	$R_1 = 0.0443$, $wR_2 = 0.0971$
R indices (all data)	$R_1 = 0.0727$, $wR_2 = 0.1114$

Table 3. Selected bond lengths [Å] and angles [°].

Bond lengths (Å)			
O(1)–Mn(1)	1.894(2)	C(1)–O(1)	1.324(2)
O(2)–Mn(1)	1.895(1)	C(7)–N(1)	1.304(3)
O(3)–Mn(1)	1.942(2)	C(14)–N(1)	1.481(2)
O(4)–Mn(1)	2.226(1)	C(16)–N(2)	1.471(3)
N(1)–Mn(1)	2.029(2)	C(19)–N(2)	1.284(2)
N(2)–Mn(1)	2.215(2)	C(21)–O(2)	1.329(2)
		C(32)–O(3)	1.324(2)
		C(38)–O(4)	1.242(2)
Bond angles (°)			
O(2)–Mn(1)–O(1)	89.64(6)	O(3)–Mn(1)–N(2)	87.19(6)
O(2)–Mn(1)–O(3)	92.80(6)	N(1)–Mn(1)–N(2)	89.94(6)
O(1)–Mn(1)–O(3)	171.04(6)	O(2)–Mn(1)–O(4)	93.76(6)
O(2)–Mn(1)–N(1)	173.59(6)	O(1)–Mn(1)–O(4)	89.34(6)
O(1)–Mn(1)–N(1)	87.07(7)	O(3)–Mn(1)–O(4)	81.90(5)
O(3)–Mn(1)–N(1)	91.28(6)	N(1)–Mn(1)–O(4)	91.70(6)
O(2)–Mn(1)–N(2)	85.33(6)	N(2)–Mn(1)–O(4)	169.00(6)
O(1)–Mn(1)–N(2)	101.61(6)		

Table 4. Hydrogen bonding and C–H... π interactions [Å, °].

Hydrogen bonds				
D–H...A	d(D–H)	d(H...A)	d(D...A)	\angle DHA
C9–H9...O3 ⁱ	0.95	2.45	3.364(2)	162
C10–H10...O2 ⁱ	0.95	2.49	3.202(3)	131
C–H... π interactions				
C–H...Cg	d(H...Cg)	d(C...Cg)	\angle CHCg	
C27–H27...Cg6 ⁱⁱ	2.95	3.609(2)	126	
C17–H17C...Cg9 ⁱ	2.74	3.682(2)	172	

Symmetry codes: ⁱ 1/2–x, 1/2+y, 1/2–z; ⁱⁱ 1/2–x, –1/2+y, 1/2–z

(N(1)), while the axial positions are occupied by carbonyl oxygen (O(4)) and nitrogen (N(2)). In most octahedral, manganese complexes of the salen-type Schiff base, the equatorial planes were generally defined by two N and two O of this ligand [6(c) and (k), 23(b)–(d), 24(a)–(d)]. As already mentioned, in this complex the four atoms (N1, N2, O2, and O1) are not coplanar, with the torsion angle \angle N1–N2–O2–O1 $-44.18(5)^\circ$. Similar arrangement of the Schiff base around Mn(III) ion is observed in complexes reported by Watkinson *et al.* [6(j)], Cheng *et al.* [8(d)] or Ha [24(e)] and is probably due to the presence of chelating ligand in the coordination sphere of a metal. Mn(III) ion lies 0.690 Å out of the mean plane formed by N1N2O2O1 of the Schiff base ligand. The equatorial atoms [N(1), O(1), O(2), and O(3)] are nearly planar with the largest deviation from the mean plane being 0.123 Å for O1. The Mn(III) center lies in the mean N(1)O(1)O(2)O(3) plane with deviation being only 0.028 Å. The equatorial bond angles at manganese(III) ion are roughly equal and close to 90° for an ideal octahedron [O(2)–Mn(1)–O(1) $89.64(6)^\circ$, O(2)–Mn(1)–O(3) $92.80(6)^\circ$, O(1)–Mn(1)–N(1) $87.07(7)^\circ$ and O(3)–Mn(1)–N(1) $91.28(6)^\circ$]. The axial bond angle [N(2)–Mn(1)–O(4) $169.00(6)^\circ$] departs significantly from linearity. It is worth noting that the axial Mn–O bond is significantly longer than the equatorial Mn–O bonds by 0.28–0.33 Å, as expected for Jahn–Teller distortion of Mn centers with a

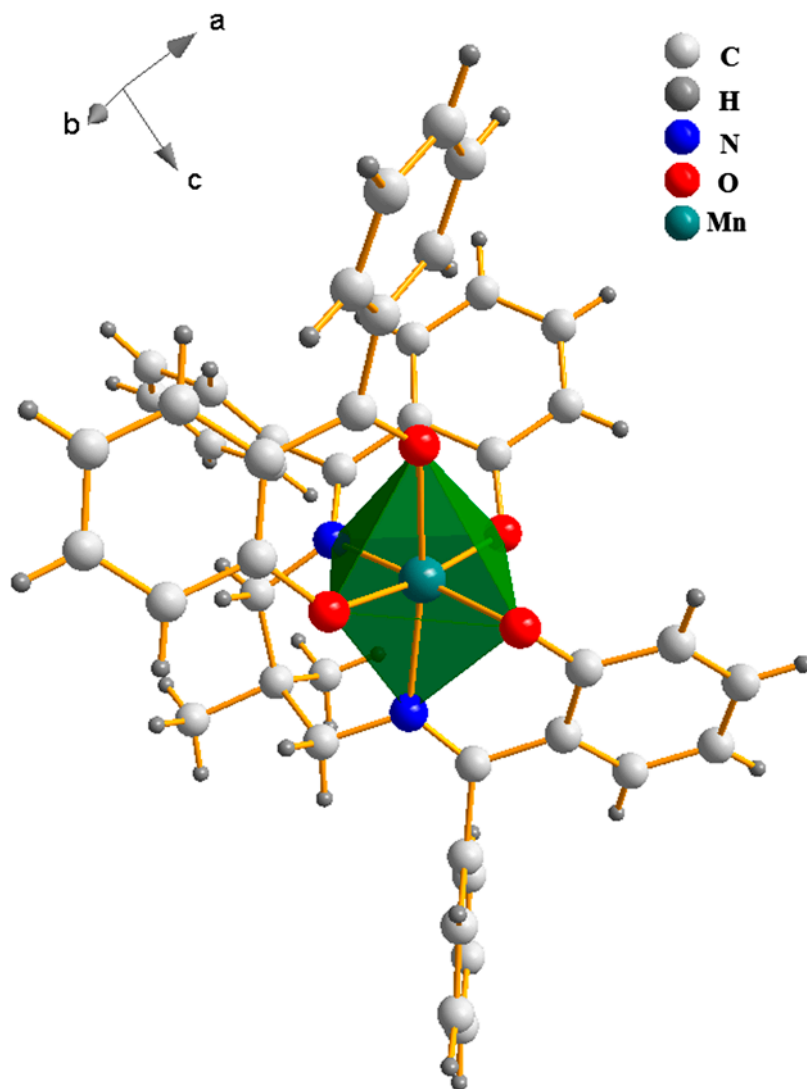


Figure 2. Coordination environment of Mn(III) ion.

+3 oxidation state [1(c), 6(c) and (i), 10(b), 16, 23(a)–(c)]. The small effect on Mn–O bond lengths can be associated with the nature of bonds as it has been suggested by Bermejo and co-workers [25]. In the case of oxygen in the equatorial plane, there is an ionic bond between the deprotonated phenol groups (negatively-charged O ions) and manganese(III) cation whereas Mn–O(4) bond is a coordination one. The short bond length C(38)–O(4) of 1.242(2) Å is equal to that in the free ketone ligand (1.240(4) Å) [20(a)] and indicates that O(4) is a ketone donor rather than a charged donor [25]. However, if we compare the present Mn(III) complex with a similar type of cobalt(III) compounds, where the Jahn–Teller effect is not observed, the differences between Co–O_{carbonyl} and Co–O_{phenoxy} bonds are less than 0.05 Å [11(b) and (c)]. This confirms that the elongation of Mn–O bond in the axial position is mainly related to the Jahn–Teller effect. All bond lengths around Mn(III) centers

are comparable to the analogs in the literature i.e. the manganese(III) Schiff base complexes with octahedral metal ion surrounded by nitrogen and oxygen donors [1(c), 6(c, f and h–j), 10(b), 16, 23(a) and (b), 26]. Coordination of Schiff base to manganese(III) does not have a significant effect on C=N bond lengths as can be seen in the complexes reported by Sang *et al.* [23(c)] or Song *et al.* [26(c)] where shortening or extending of azomethine bond length was observed. The C=N bond distances are 1.284(2) and 1.304(3) Å in **2** and 1.289(3) and 1.296(3) Å in the free Schiff base [18]. The Schiff base ligand is tetradentate, forming three fused six-membered chelate rings (A: Mn/O1/C1/C6/C7/N1; B: Mn/N1/C14/C15/C16/N2; C: Mn/O2/C21/C20/C19/N2) around manganese(III), while the ketone is bidentate, also forming a six-membered ring (D: Mn/O3/C32/C37/C38/O4). The A ring presents intermediate conformation between envelope and screw-boat with the Cremer–Pople parameter $Q = 0.623(1)$ Å, $\theta = 64.4(2)^\circ$ and $\varphi = 15.4(2)^\circ$. The B ring adopts a chair conformation [$Q = 0.606(2)$ Å, $\theta = 3.7(2)^\circ$ and $\varphi = 193(3)^\circ$] while the C and D rings form distorted screw-boats ($Q = 0.652(2)$ Å, $\theta = 68.3(2)^\circ$ and $\varphi = 28.8(2)^\circ$ for C; $Q = 0.452(2)$ Å, $\theta = 70.3(2)^\circ$ and $\varphi = 29.7(2)^\circ$ for D) [27].

There are no strong hydrogen bonds and the structure is stabilized by weak intermolecular C–H...O hydrogen bonds and C–H... π (ring) interactions. Hydrogens of the benzene ring interact with phenolic oxygens of neighboring molecules through a pair of C_{ar}–H...O hydrogen bonds, forming a cyclic hydrogen bonded motif with the graph set notation, $R_2^2(7)$. C_{ar}–H...O hydrogen bonds are found between C9–H9...O3ⁱ and C10–H10...O2ⁱ [symmetry code (i): $1/2 - x, 1/2 + y, 1/2 - z$ (table 4)]. The lengths of these interactions (C...O) are 3.364(2) and 3.202(3) Å and on the basis of geometric considerations they can be classified as weak hydrogen bonds [28]. Intermolecular C–H...Cg contacts (table 4, figure 3) occur between centroids of the two phenyl rings (Cg6 and Cg9, centroid of the phenyl formed by C8–C13 and C32–C37) and phenyl hydrogen [C27–H27...Cg6ⁱⁱ, symmetry code (ii): $1/2 - x, -1/2 + y, 1/2 - z$] and methyl hydrogen [C17–H17C...Cg9ⁱ, symmetry code (i): $1/2 - x, 1/2 + y, 1/2 - z$]. The distances of C–H...Cg contacts are 3.609(2) Å for C27–H27...Cg6 and 3.682(2) Å for C17–H17C...Cg9. The intermolecular C–H...O hydrogen bonds and C–H... π (ring) interactions link the molecules into chains running parallel to the [0 1 0] direction (see figure 3). Due to these supramolecular interactions, the Mn...Mn distance of 7.955 Å is too long to establish intermetallic interactions between neighboring manganese ions. Similar to the related compounds reported by Biswas *et al.*

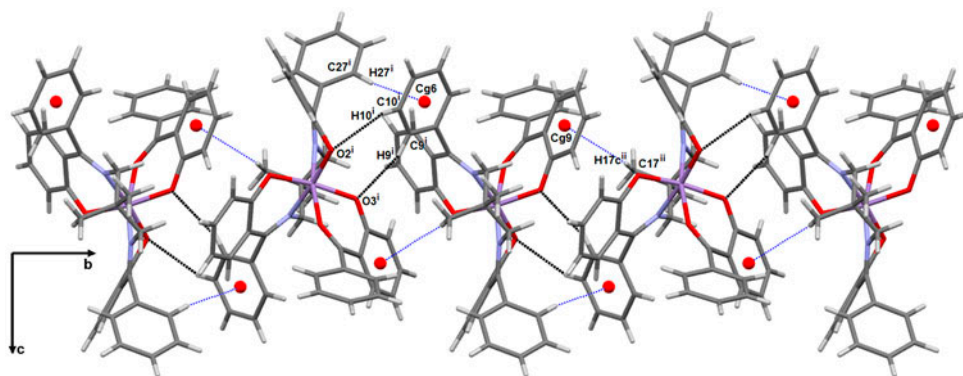


Figure 3. Part of the crystal structure of manganese(III) complex showing C–H...O hydrogen bonds and C–H... π (ring) interactions as well as formation of 1-D chains along the *b*-axis.

[29], the lack of bridging ligands [6(f and h), 26(b)] rather excludes any kind of exchange interaction between manganese(III) ions, which confirms the result of the magnetic study.

3.3. Electronic absorption spectra

The electronic absorption spectra data of **1** and ligands in protic and aprotic solvents are summarized in table S3 and shown in figures S6–S11 (Supplementary data). The UV–vis spectra of the Schiff base depend on the type of solvent used. The spectrum of free Schiff base exhibits five (in protic solvents) or three bands (in aprotic solvents, except the spectrum recorded in DMF). The bands which are observed in the range 209–229 nm and 258–286 nm can originate from $\pi \rightarrow \pi^*$ transitions of the aromatic ring. The next band at 324–325 nm is due to $\pi \rightarrow \pi^*$ transition of the azomethine group [16, 30]. Similar to other Schiff bases [16, 30(c), 31], in protic solvents at 400–403 nm the band originating from $n \rightarrow \pi^*$ transition of the azomethine group is also observed. The appearance of the additional band in polar protic solvents provides information about enolimine–ketoamine tautomerism of the Schiff base ligand. In polar aprotic solvents, like in the solid state [18], the ligand is present predominantly as enolimine. According to the literature [16, 31], the additional band at 400–403 nm can be linked with the shift of the tautomeric equilibrium to the ketoamine form. The intensity of this band increases with polarity of solvent used. This confirms the stabilization of the more polar ketoamine form in the more polar solvent, which was also observed for other Schiff bases [16, 30(c), 31]. UV–vis spectra of K ligand in different solvents contain three bands (except the spectrum recorded in DMF). Similarly for SchB ligand, the bands at 210–219 nm and 260–270 nm are due to $\pi \rightarrow \pi^*$ transitions of the aromatic ring. The bands at 334–339 nm originate from $n \rightarrow \pi^*$ transition in the carbonyl group [31(a) and (b), 32]. The spectra of metal compounds contain bands characteristic of both ligand and metal ion [16]. In the complex, the intense absorption bands at 204–237 and 260–283 nm can be assigned to intraligand $\pi \rightarrow \pi^*$ transitions which are typical of complexes with this type of ligand [16, 30(c), 33]. Mn(III) complexes with octahedral geometry often show one charge transfer band around 400 nm and a spin allowed d–d transition band around 500 nm. In the studied complex, the charge transfer band is shifted to a lower wavelength (358–367 nm) and is observed for the spectra recorded in protic and DMF solvents. This band can be attributed to the phenolate $O(p_\pi) \rightarrow Mn(d_{\pi^*})$ ligand-to-metal charge transfer by analogy with related manganese(III) complexes combined with $n \rightarrow \pi^*$ transitions of (C=N) and (C=O) [16, 33]. Similarly to the previously described manganese(III) complex [16], the band characteristic of d–d transition is not observed in the spectrum of the studied compound at the concentration used. In more concentrated solutions ($1 \times 10^{-3} \text{ mol L}^{-1}$), this band appears as a shoulder *ca.* 500–540 nm.

Additionally, we calculated UV–vis spectra using the CIS HF, CIS DFT, and TD DFT methods. For the purpose of UV–vis spectra calculations, the energy and geometry of the ketone, Schiff base, and the complex were first optimized in solvents using the Polarizable Continuum Model solvent model [34(a)]. This approach creates a solute cavity via a set of overlapping spheres. In the case of MeOH:H₂O (1:1 v/v) mixture, it was assumed that solvent component descriptors vary linearly; thus, a linear combination of their values may be used [34(b)]. The values of dielectric constants used in computations were 78.3900 for water and 32.6130 for methanol, thus the dielectric constant for a mixture of 0.6919 M fraction of water (assuming density of 1.00 g cm^{-3}) and 0.3081 M fraction of methanol

(assuming density 0.7918 g cm^{-3}) yields 64.2860. The UV–vis spectra were calculated with the configuration interaction singles (CIS) method [34(c)] for HF- and B3LYP-optimized structures and time-dependent (TD) approach [34(d)] for B3LYP-optimized structures. The dielectric constants at infinite frequency, required for the excited state calculation, were 1.7760 for water and 1.7580 for methanol, yielding the value of this parameter 1.7704 for the mixture. Surprisingly, the CIS method resulted in better approximation than the TD DFT approach. The UV–vis spectra were enhanced by a scaling procedure according to the scaling factors as previously reported [34(e)]. We proposed scaling factors for a given basis set, separately for each method and each compound (table 5). The proposed scaling factors are comparable to those reported by Suendo and Viridi [34(e)]. The inaccuracy of the computed UV–vis spectra for the complex may be caused by insufficient basis set or insufficient theory level.

3.4. Thermal analysis (TG/DSC and TG/FTIR)

Thermal analyses of the complexes were made by the TG/DSC (air, for **1** and **2**) and TG/FTIR (nitrogen, for **1**) techniques. The thermoanalytical curves TG/DTG and DSC for **1** and **2** are presented in figure 4. Complexes **1** and **2** are stable at room temperature. The first changes in the mass on TG curves (endothermic peak on DSC) of **1** are found above $37 \text{ }^\circ\text{C}$ (for air) and $35 \text{ }^\circ\text{C}$ (for nitrogen). The observed mass losses for this step are 4.13 and 4.53%, respectively, for air and nitrogen analysis. The values are similar, indicating that the first stage is probably the same in both cases and is related to the release of methanol (Calcd value 4.30%). The desolvation process is connected with an endothermic effect recorded on the DSC curve of **1**. The enthalpy of this process is equal to $34.4 \pm 0.1 \text{ kJ mol}^{-1}$. The first stage, the desolvation process, is also reflected on the FTIR spectra of the evolved gasses phase. The characteristic vibration bands of CH_3OH appear at $3750\text{--}3600$, $3150\text{--}2750$, and $1100\text{--}950 \text{ cm}^{-1}$ [16, 35], which confirms the presence of solvent molecules in the crystal structure of the polycrystalline complex. Further thermal decomposition of **1** in air takes place in a similar way to that of **2** and includes three stages during which destruction and combustion of ligands are observed. In the first two stages of ligand decomposition, which occur between $123\text{--}183 \text{ }^\circ\text{C}$ and $188\text{--}345 \text{ }^\circ\text{C}$, intermediate, unstable products are formed; the weight losses are 8.37 and 25.35% for **1** and 3.21 and 21.36% for **2**. The last stage above $\sim 350 \text{ }^\circ\text{C}$ corresponds to complete destruction and combustion of the remaining parts of the ligands and formation of a final product which can be MnO_2 (found and calculated total weight losses are 88.24 and 88.33% for **1**; 87.80 and 87.81% for **2**), similar to thermal decomposition of complexes reported by Filho *et al.* and Goher *et al.* [36].

In nitrogen atmosphere, thermal decomposition of **1** occurs at the beginning as in air (figure 4). The step between 120 and $174 \text{ }^\circ\text{C}$ is assigned to destruction and combustion of the ligands. The experimental weight loss of this level is 9.36%. This stage is connected with the release of CO_2 , CO , and NO and methyl isocyanate. The bands' characteristic of carbon dioxide is at $2450\text{--}2300 \text{ cm}^{-1}$ and $750\text{--}600 \text{ cm}^{-1}$ due to valence and deformation

Table 5. Scaling factors for improvement of calculated UV–vis spectra.

Compound	Schiff base			Ketone			Complex		
	CIS HF	CIS DFT	TD DFT	CIS HF	CIS DFT	TD DFT	CIS HF	CIS DFT	TD DFT
Scaling factor	0.9276	0.8995	0.8735	0.9213	0.8877	0.9082	0.5360	0.5468	0.4924

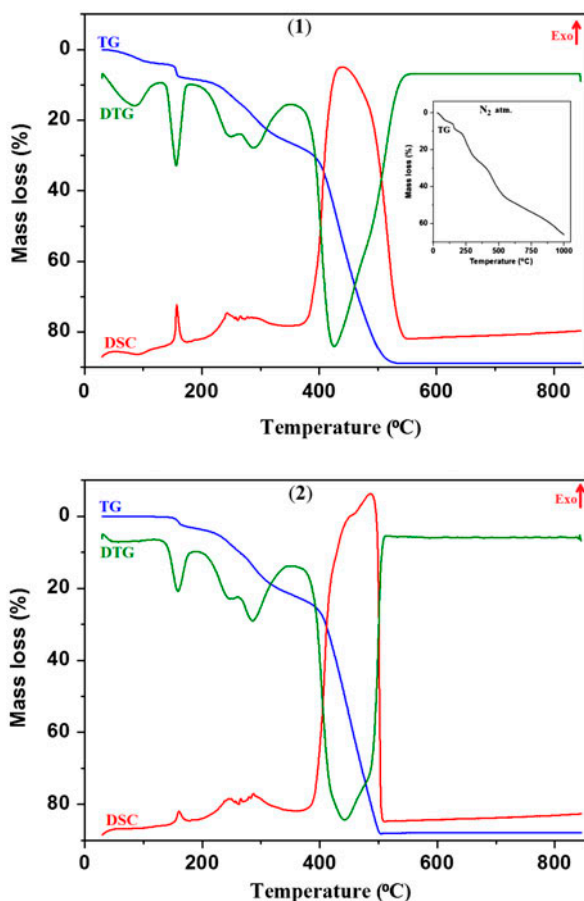
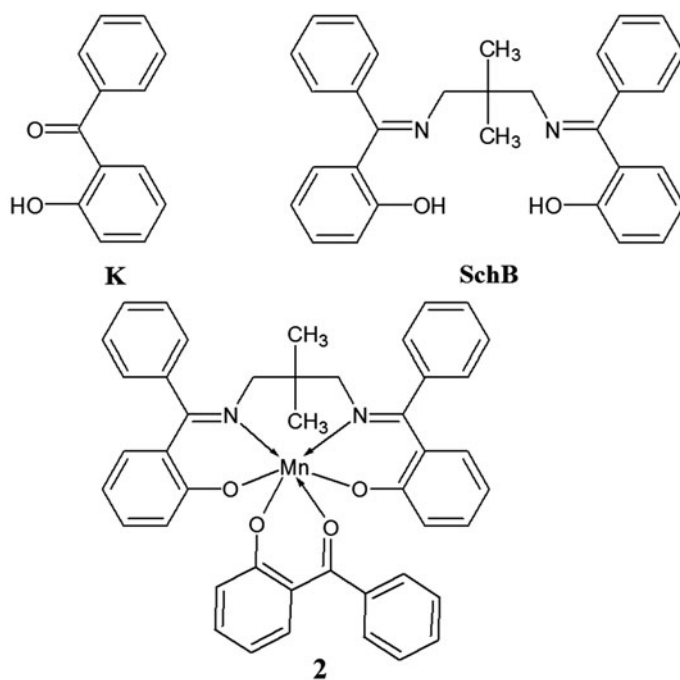


Figure 4. TG, DTG and DSC curves for **1** and **2** in air and TG curve in nitrogen.

vibrations, respectively. The double peaks corresponding to CO are at $2275\text{--}2050\text{ cm}^{-1}$. The bands with the maxima which appear between peaks characteristic of CO_2 and CO (2311 , 2305 and 2294 cm^{-1}) are probably due to methyl isocyanate. The weak bands corresponding to NO are recorded at $1950\text{--}1750\text{ cm}^{-1}$ with a characteristic peak at 1875 cm^{-1} [1(b), 16, 35]. The next stage on the TG curve is at $180\text{--}340\text{ }^\circ\text{C}$ with the mass loss 25.87%. During this interval, destruction and combustion of the next part of the ligands are observed and an unstable product is formed. The gaseous products recorded on FTIR spectra are: CO_2 , NH_3 , CH_4 , and methyl isocyanate. Major bands for NH_3 are observed at $750\text{--}1200\text{ cm}^{-1}$ with the characteristic double-peak bands of the maxima at 965 and 931 cm^{-1} . The weak bands characteristic of CH_4 (in the range $3175\text{--}2900\text{ cm}^{-1}$ with the characteristic maximum at 3016 cm^{-1}) appeared at the end of this stage about $290\text{ }^\circ\text{C}$ [1(b), 16, 35, 37]. The intermediate, formed during this stage, is unstable and immediately undergoes further decomposition. The experimental weight loss of this stage is equal to 48.04%. The gaseous products released during this step are similar to those observed in the previous one with more intense bands corresponding to the presence of methane. The methane bands disappear at $560\text{ }^\circ\text{C}$. The last stage above $600\text{ }^\circ\text{C}$ corresponds to the final destruction and



Scheme 1. Ketone (K) and Schiff base (SchB) ligands and manganese(III) complex in the single-crystal (**2**) form.

combustion of ligands. At the beginning of this step, CO₂ and methyl isocyanate were observed on FTIR spectra. At a higher temperature (*ca.* 820 °C), the peaks characteristic of CO are recorded. It can be observed from the TG curve that the decomposition process was not completed in nitrogen.

4. Conclusion

We synthesized and characterized a manganese(III) complex ([Mn(C₃₁H₂₈N₂O₂)(C₁₃H₉O₂)]·CH₃OH (**1**). During the synthesis of **1**, we expected that Mn(II) would be oxidized to Mn(III) and the metal center would be coordinated through a tetradentate Schiff base, solvent molecules, or/and nitrate ion similar to previously reported manganese complex [16]. Surprisingly the Schiff base is partially hydrolyzed and one of its products, the ketone, has coordinated to manganese(III). Compound **1** was obtained as an amorphous powder containing solvent in the structure ([Mn(C₃₁H₂₈N₂O₂)(C₁₃H₉O₂)]·CH₃OH). After slow recrystallization at low temperature (4 °C) a few single crystals were obtained. X-ray analysis has revealed that after recrystallization methanol molecules were not incorporated into the crystal lattice ([Mn(C₃₁H₂₈N₂O₂)(C₁₃H₉O₂)] (**2**). Thermal decomposition of **1** and **2**, after desolvation of the amorphous complex, takes place in the same way which can indicate that there is the same coordination environment around manganese(III) (i.e. through two phenoxo oxygens and two imine nitrogens from the Schiff base ligand and two oxygens from ketone) in both forms. It should be also noted that in polar solvents (MeOH, EtOH)

and DMF, ketone is probably replaced by appropriate solvent molecules causing the complex to behave like a uni-univalent electrolyte.

Supplementary material

Crystallographic data have been deposited with the CCDC, 12 Union Road, Cambridge, CB2 1EZ, UK (Fax: +44 1223 366033; Email: deposit@ccdc.cam.ac.uk or [www://www.ccdc.cam.ac.uk](http://www.ccdc.cam.ac.uk)) and are available on request, quoting the deposition number CCDC 1007872.

Acknowledgements

The presented research was partially performed during the postdoctoral stay of Agnieszka A. Kaczor at the University of Eastern Finland, Kuopio, Finland, under a Marie Curie fellowship. Calculations were made under a computational grant from the Interdisciplinary Center of Mathematical and Computational Modelling (ICM) in Warsaw, Poland, grant number G30-18 and under resources and licenses of CSC, Finland.

Disclosure statement

No potential conflict of interest was reported by the authors.

Funding

This work was supported by the Interdisciplinary Center of Mathematical and Computational Modelling (ICM) in Warsaw, Poland [grant number G30-18].

References

- [1] (a) K. Ghosh, N. Tyagi, P. Kumar, U.P. Singh, N. Goel. *J. Inorg. Biochem.*, **104**, 9 (2010); (b) Z. Rzączyńska, A. Bartyzel, T. Głowiak. *Polyhedron*, **22**, 2595 (2003); (c) M. Maiti, D. Sadhukhan, S. Thakurta, E. Zangrando, G. Pilet, A. Bauzá, A. Frontera, B. Dede, S. Mitra. *Polyhedron*, **75**, 40 (2014); (d) D. Lieb, I. Kenkell, J. Lj. Miljković, D. Moldenhauer, N. Weber, M.R. Filipović, F. Gröhn, I. Ivanović-Burmazović. *Inorg. Chem.*, **53**, 1009 (2014).
- [2] (a) D. Čechová, A. Martišková, Z. Padělková, L. Gal'a, L. Dlhán, D. Valigura, M. Valko, R. Boča. *J. Moncol Polyhedron*, **79**, 129 (2014); (b) V. Chandrasekhar, J. Goura, K. Gopal, J. Liu, P. Goddard. *Polyhedron*, **72**, 35 (2014); (c) Y. Wang, H. Zhou, X. Shena, A. Yuan. *Inorg. Chim. Acta*, **414**, 53 (2014).
- [3] (a) A.S. Roy, M.K. Biswas, T. Weyhermuller, P. Gho. *Dalton Trans.*, **40**, 146 (2011); (b) A. Sood, M.T. Räisänen, E. Aitola, A. Sibaoui, E. Colacio, M. Ahlgren, M. Nieger, T. Repo, M. Leskelä. *Polyhedron*, **56**, 221 (2013).
- [4] (a) M. Zampakou, M. Akrivou, E.G. Andreadou, C.P. Raptopoulou, V. Psycharis, A.A. Pantazaki, G. Psomas. *J. Inorg. Biochem.*, **121**, 88 (2013); (b) D.P. Singh, K. Kumar, C. Sharma. *Eur. J. Med. Chem.*, **45**, 1230 (2010); (c) S. Mandal, T.K. Karmakar, A. Ghosh, M. Fleck, D. Bandyopadhyay. *Polyhedron*, **30**, 790 (2011).
- [5] N. Noshiranzadeh, M. Emami, R. Bikas, K. Ślepokura, T. Lis. *Polyhedron*, **72**, 56 (2014).
- [6] (a) S. Biswas, K. Mitra, S.K. Chattopadhyay, B. Adhikary, C.R. Lucas. *Transition Met. Chem.*, **30**, 393 (2005); (b) G.E. Kostakis, A.M. Akoa, A.K. Powell. *Chem. Soc. Rev.*, **39**, 2238 (2010); (c) P. Seth, M.G.B. Drew, A. Ghosh. *J. Mol. Catal. A: Chem.*, **365**, 154 (2012); (d) C.C. Stoumpos, T.C. Stamatatos, H. Sartz,

- O. Roubeau, A.J. Tasiopoulos, V. Nastopoulos, S.J. Teat, G. Christou, S.P. Perlepes. *Dalton Trans.*, 1004 (2009); (e) C. Hureau, E. Anxolabéhère-Mallart, M. Nierlich, F. Gonnet, E. Rivière, G. Blondin. *Eur. J. Inorg. Chem.*, **2002**, 2710 (2002); (f) D.J. Darensbourg, E.B. Frantz. *Inorg. Chem.*, **47**, 4977 (2008); (g) M.R. Maurya, P. Saini, C. Haldar, F. Avecilla. *Polyhedron*, **31**, 710 (2012); (h) Y. Yahsi, H. Kara. *Spectrochim. Acta, Part A*, **127**, 25 (2014); (i) H. Kargar. *Transition Met. Chem.*, **39**, 811 (2014); (j) M. Watkinson, M. Fondo, M.R. Bermejo, A. Sousa, C.A. McAuliffe, R.G. Pritchard, N. Jaiboon, N. Aurangzeb, M. Naeem. *J. Chem. Soc., Dalton Trans.*, 31–41 (1999); (k) M.R. Bermejo, M. Fondo, A. García-Deibe, A.M. González, A. Sousa, J. Sanmartín, C.A. McAuliffe, R.G. Pritchard, M. Watkinson, V. Lukov. *Inorg. Chim. Acta*, **293**, 210 (1999).
- [7] (a) J.D. Harvey, C.J. Ziegler. *J. Inorg. Biochem.*, **100**, 869 (2006); (b) S. Signorella, C. Hureau. *Coord. Chem. Rev.*, **256**, 1229 (2012); (c) L. Shivakumar, K. Shivaprasad, H.D. Revanasiddappa. *Spectrochim. Acta, Part A*, **107**, 203 (2013); (d) C.S. Mullins, V.L. Pecoraro. *Coord. Chem. Rev.*, **252**, 416 (2008); (e) M. Maneiro, M.R. Bermejo, M.I. Fernández, E. Gómez-Fórneas, A.M. González-Noya, A.M. Tyryshkin. *New J. Chem.*, **27**, 727 (2003).
- [8] (a) K. Fujisawa, M. Nabika. *Coord. Chem. Rev.*, **257**, 119 (2013); (b) I. Kuźniarska-Biernacka, O. Rodrigues, M.A. Carvalho, P. Parpot, K. Biernacki, A.L. Magalhães, A.M. Fonseca, I.C. Neves. *Eur. J. Inorg. Chem.*, **2013**, 2768 (2013); (c) L. Ma, F. Su, X. Zhang, D. Song, Y. Guo, J. Hu. *Microporous Mesoporous Mater.*, **184**, 37 (2014); (d) M.-C. Cheng, M.C.-W. Chan, S.-M. Peng, K.-K. Cheung, C.-M. Che. *J. Chem. Soc., Dalton Trans.*, 3479 (1997); (e) A. Aghmiza, N. Mostfa, S. Iksi, R. Rivas, M.D. González, Y. Diaz, F. El Guemmout, A. El Laghdach, R. Echarri, A.M. Masdeu-Bultó. *J. Coord. Chem.*, **66**, 2567 (2013).
- [9] (a) G. Tang, S. Kou, Z. Zhang, T. Tang, L.F. Culnane, Y. Zhang, Y. Song. *Synth. Met.*, **182**, 60 (2013); (b) A.G. Bezerra Jr., I.E. Borissevitch, R.E. de Araujo, A.S.L. Gomes, C.B. de Araújo. *Chem. Phys. Lett.*, **318**, 511 (2000).
- [10] (a) O. Roubeau, R. Clérac. *Eur. J. Inorg. Chem.*, **2008**, 4325 (2008); (b) S. Richeter, J. Larionova, J. Long, A. van der Lee, D. Leclercq. *Eur. J. Inorg. Chem.*, **2013**, 3206, (2013).
- [11] (a) C. Fukuhara, S. Matsuda, K. Katsura, M. Mori, K. Matsumoto, S. Ooi, Y. Yoshikawa. *Inorg. Chim. Acta*, **142**, 203 (1988); (b) S.K. Gupta, P.B. Hitchcock, G.S. Argal. *Inorg. Chim. Acta*, **361**, 2139 (2008); (c) R. Kia, H. Kargar, K. Zare, I.U. Khan. *Acta Cryst.*, **E66**, m366 (2010).
- [12] (a) R.S. Black, D.G. Billing, A. Bartyzel, E.M. Cukrowska. *Acta Cryst.*, **E66**, o1256 (2010); (b) R.S. Black, D.G. Billing, A. Bartyzel, E.M. Cukrowska. *Acta Cryst.*, **E66**, o1002 (2010).
- [13] (a) G.A. Bain, J.F. Berry. *J. Chem. Educ.*, **85**, 532 (2008); (b) K. Burger. *Coordination Chemistry: Experimental Methods*, Akademia Kiadó, Budapest (1973).
- [14] (a) Oxford Diffraction, Xcalibur CCD System, CrysAlis Software System, Version 1.171, Oxford Diffraction Ltd, Abingdon (2009); (b) G.M. Sheldrick. *Acta Cryst., Sect. A*, **64**, 112 (2008); (c) L.J. Farrugia. *J. Appl. Crystallogr.*, **32**, 837 (1999); (d) L.J. Farrugia. *J. Appl. Cryst.*, **45**, 849 (2012); (e) C.F. Macrae, P.R. Edgington, P. McCabe, E. Pidcock, G.P. Shields, R. Taylor, M. Towler, J. van de Streek. *J. Appl. Cryst.*, **39**, 453 (2006); (f) K. Brandenburg, H. Putz. *Diamond – Crystal and Molecular Structure Visualization*, Crystal Impact GbR, Bonn, Germany (1999); (g) A.L. Spek. *J. Appl. Cryst.*, **36**, 7 (2003).
- [15] (a) A. Becke. *J. Chem. Phys.*, **98**, 5648 (1993); (b) C. Lee, W. Yang, R.G. Parr. *Phys. Rev. B*, **37**, 785 (1988); (c) Gaussian 09, Revision A.1, M.J. Frisch, G.W. Trucks, H.B. Schlegel, G.E. Scuseria, M.A. Robb, J.R. Cheeseman, G. Scalmani, V. Barone, B. Mennucci, G.A. Petersson, H. Nakatsuji, M. Caricato, X. Li, H.P. Hratchian, A.F. Izmaylov, J. Bloino, G. Zheng, J.L. Sonnenberg, M. Hada, M. Ehara, K. Toyota, R. Fukuda, J. Hasegawa, M. Ishida, T. Nakajima, Y. Honda, O. Kitao, H. Nakai, T. Vreven, J.A. Montgomery Jr., J.E. Peralta, F. Ogliaro, M. Bearpark, J.J. Heyd, E. Brothers, K.N. Kudin, V.N. Staroverov, R. Kobayashi, J. Normand, K. Raghavachari, A. Rendell, J.C. Burant, S.S. Iyengar, J. Tomasi, M. Cossi, N. Rega, J.M. Millam, M. Klene, J.E. Knox, J.B. Cross, V. Bakken, C. Adamo, J. Jaramillo, R. Gomperts, R.E. Stratmann, O. Yazyev, A.J. Austin, R. Cammi, C. Pomelli, J.W. Ochterski, R.L. Martin, K. Morokuma, V.G. Zakrzewski, G.A. Voth, P. Salvador, J.J. Dannenberg, S. Dapprich, A.D. Daniels, O. Farkas, J.B. Foresman, J.V. Ortiz, J. Cioslowski, D.J. Fox. Gaussian Inc., Wallingford (2009); (d) B. Trzaskowski, A. Les, L. Adamowicz. *Int. J. Mol. Sci.*, **4**, 503 (2003); (e) Dassault Systèmes BIOVIA. *Discovery Studio Modeling Environment, Release 3.1*, Dassault Systèmes, San Diego, USA (2015); (f) A.R. Allouche. *J. Comput. Chem.*, **32**, 174 (2011); (g) ChemCraft v. 1.7 software. Available on at: <http://www.chemcraftprog.com>; (h) M.H. Jamróz. *Vibrational Energy Distribution Analysis VEDA 4*, Warsaw (2004); (i) M.H. Jamróz. *Spectrochim. Acta, Part A*, **114**, 220 (2013); (j) Y. Sert, M. Mahendra, S. Keskinoglu, Chandra, N. Srikantamurthy, K.B. Umehsa, Ç. Çirak. *Spectrochim. Acta, Part A*, **139**, 145 (2015); (k) U. Gupta, V. Kumar, V.K. Singh, R. Kant, Y. Khajuria. *Spectrochim. Acta, Part A*, **140**, 65 (2015); (l) M. Suhasini, E. Sailatha, S. Gunasekaran, G.R. Ramkumaar. *Spectrochim. Acta, Part A*, **141**, 252 (2015); (m) Chemission v. 4.01 demo version. Available online at: <http://www.chemission.com>.
- [16] A. Bartyzel. *J. Coord. Chem.*, **66**, 4292 (2013).
- [17] W.J. Geary. *Coord. Chem. Rev.*, **7**, 81 (1971).
- [18] J.P. Corden, W. Errington, P. Moore, P.R. Phillips, M.G.H. Wallbridge. *Acta Cryst.*, **C52**, 3199 (1996).
- [19] (a) H.H. Freedman. *J. Am. Chem. Soc.*, **83**, 2900 (1961); (b) K. Ueno, A.E. Martell. *J. Phys. Chem.*, **59**, 998 (1955); (c) W. Zieliński, A. Rajca. *Spectroscopic Methods and their Applications for the Organic Compound Identifications*, Scientific and Technical Publisher, Warsaw (2000).

- [20] (a) K. Saraswat, R.N. Prasad, R. Ratnani, J.E. Drake, M.B. Hursthouse, M.E. Light. *Inorg. Chim. Acta*, **359**, 1291 (2006); (b) B. Zhang, T. Xiao, C. Liu, Q. Li, Y. Zhu, M. Tang, C. Du, M. Song. *Inorg. Chem.*, **52**, 13332 (2013).
- [21] B. Cristóvão, B. Mirosław. *Inorg. Chim. Acta*, **401**, 50 (2013).
- [22] (a) M. Pitucha, Z. Karczmarzyk, W. Wysocki, A.A. Kaczor, D. Matosiuk. *J. Mol. Struct.*, **994**, 313 (2011); (b) N. Özdemir, M. Dinçer, A. Çukurovalı, O. Büyükgüngör. *J. Mol. Model.*, **15**, 1435 (2009); (c) A. Kaczor, R. Almeida, A. Gomez-Zavaglia, M. de Lurdes, S. Cristiano, R. Fausto. *J. Mol. Struct.*, **876**, 77 (2008); (d) M.P. Andersson, P. Uvdal. *J. Phys. Chem. A*, **109**, 2937 (2005).
- [23] (a) I.-C. Hwang, K. Ha. *Acta Cryst.*, **E63**, m2337 (2007); (b) Y. Zhou, J.-N. Peng. *J. Coord. Chem.*, **66**, 2597 (2013); (c) Y.-L. Sang, X.-C. Li, W.-M. Xiao. *J. Coord. Chem.*, **66**, 4015 (2013); (d) Z.-W. Li, P.-P. Yang, X.-L. Wang, L.-C. Li. *J. Coord. Chem.*, **63**, 1538 (2010).
- [24] (a) S. Lin, Q. Wu, H. Tan, E. Wang. *J. Coord. Chem.*, **64**, 3661 (2011); (b) P.P. Chakrabarty, S. Saha, D. Schollmeyer, A.K. Boudalis, A.D. Jana, D. Luneau. *J. Coord. Chem.*, **66**, 9 (2013); (c) I.-C. Hwang, K. Ha. *Z. Kristallogr. NCS*, **221**, 363 (2006); (d) I.-C. Hwang, K. Ha. *Z. Kristallogr. NCS*, **221**, 365 (2006); (e) K. Ha. *Z. Kristallogr. NCS*, **225**, 257 (2010); (f) M.-C. Cheng, M.C.-W. Chan, S.-M. Peng, K.-K. Cheung, C.-M. Che. *J. Chem. Soc., Dalton Trans.*, 3479, (1997).
- [25] M.R. Bermejo, A.G. Deibe, M. Rey, J. Sanmartin, A. Sousa, N. Aurangzeb, C.E. Hulme, C.A. McAuliffe, R.G. Pritchard, M. Watkinson, M. Helliwell. *J. Chem. Soc., Dalton Trans.*, 1265, (1994).
- [26] (a) M.Á. Vázquez-Fernández, M.I. Fernández-García, A.M. González-Noya, M. Maneiro, M.R. Bermejo, M.J. Rodríguez-Doutón. *Polyhedron*, **31**, 379 (2012); (b) P. Kar, R. Biswas, M.G.B. Drew, Y. Ida, T. Ishida, A. Ghosh. *Dalton Trans.*, **40**, 3295 (2011); (c) J.H. Song, K.S. Lim, D.W. Ryu, S.W. Yoon, B.J. Suh, C.S. Hong. *Inorg. Chem.*, **53**, 7936 (2014).
- [27] (a) D. Cremer, J.A. Pople. *J. Am. Chem. Soc.*, **97**, 1354 (1975); (b) J.C.A. Boeyens. *J. Cryst. Mol. Struct.*, **8**, 317 (1978); (c) P.J. Pérez, R. Carrascosa, L. García, G. Barandika, A. Calderón-Casado, E. Pérez, J.L. Serrano, M.D. Santana. *Dalton Trans.*, **40**, 9504 (2011); (d) K. Kubono, K. Tani, K. Yokoi, T. Shinmyozu, K. Gotob. *Acta Cryst.*, **E69**, m629 (2013).
- [28] G.R. Desiraju, T. Steiner. *The Weak Hydrogen Bond in Structural Chemistry and Biology*, Oxford University Press Inc., New York (1999).
- [29] S. Biswas, T. Kar, S. Sarkar, K. Dey. *J. Coord. Chem.*, **65**, 980 (2012).
- [30] (a) L.D.S. Yadav. *Organic Spectroscopy*, Kluwer Academic Publisher, New Delhi (2005); (b) C.N.R. Rao. *Ultra-Violet and Visible Spectroscopy. Chemical application*, PWN, Warsaw (1980); (c) B. Bosnich. *J. Am. Chem. Soc.*, **90**, 627 (1968).
- [31] (a) P. Jeslin, K. Inba, B. Annaraj, S. Thalamuthu, M.A. Neelakantan. *Spectrochim. Acta, Part A*, **104**, 300 (2013); (b) N. Galić, Z. Cimerman, V. Tomišić. *Spectrochim. Acta, Part A*, **71**, 1274 (2008).
- [32] (a) K. Chaitanya. *Spectrochim. Acta, Part A*, **86**, 159 (2012); (b) S.E. Blanco, E.I. Gasull, F.H. Ferretti. *Spectrochim. Acta, Part A*, **59**, 2985 (2003).
- [33] (a) A. Neves, S.M.D. Erthal, I. Vencato, A.S. Ceccato, Y. Mascarenhas, O.R. Nascimento, M. Horner, A.A. Batista. *Inorg. Chem.*, **31**, 4749 (1992); (b) D. Moreno, V. Daier, C. Palopoli, J.-P. Tuchagues, S. Signorella. *Inorg. Biochem.*, **104**, 496 (2010); (c) W. Shi, Y. Liu, B. Liu, Y. Song, Y. Xu, H. Wang, Y. Sha, G. Xu, S. Styring, P. Huang. *J. Coord. Chem.*, **59**, 119 (2006).
- [34] (a) S. Miertuš. *J. Tomasi. Chem. Phys.*, **65**, 239 (1982); (b) M. Makarska-Bialokoz, A.A. Kaczor. *Spectrosc. Lett.*, **47**, 147 (2014); (c) J.B. Foresman, Æ. Frisch. *Exploring Chemistry with Electronic Structure Methods*, 2nd Edn, Gaussian Inc, Pittsburgh (1996); (d) R. Bauernschmitt, R. Ahlrichs. *Chem. Phys. Lett.*, **256**, 454 (1996); (e) V. Suendo, S. Viridi. *ITB J. Sci.*, **44A**, 93 (2012).
- [35] A. Dzielulska-Kułażkowska, A. Bartyzel. *J. Mol. Struct.*, **1033**, 67 (2013).
- [36] (a) C. Filho, M.A. da Silva, I. Massao. *Eclat. Quím.*, **23**, 9 (1998); (b) M.A.S. Goher, A.K. Hafez, M.A.M. Abu-Youssef, A.M.A. Badr, C. Gspan, F.A. Mautner. *Polyhedron*, **23**, 2349 (2004).
- [37] Z. Rzączyńska, A. Bartyzel, T. Głowiak. *J. Coord. Chem.*, **56**, 77 (2003).